

## Article

# Tracking and Evaluating the Concentrations of Natural Radioactivity According to Chemical Composition in the Precambrian and Mesozoic Granitic Rocks in the Jangsu-gun Area, Central Southwestern South Korea

Sung Won Kim <sup>1</sup>, Weon-Seo Kee <sup>1,\*</sup>, Saro Lee <sup>2</sup>, Byung Choon Lee <sup>1</sup> and Uk Hwan Byun <sup>1</sup>

<sup>1</sup> Geology Division, Korea Institute of Geoscience and Mineral Resources, 124, Gwahak-ro Yuseong-gu, Daejeon 34132, Korea; sungwon@kigam.re.kr (S.W.K.); lbc@kigam.re.kr (B.C.L.); buh@kigam.re.kr (U.H.B.)

<sup>2</sup> Geoscience Platform Research Division, Korea Institute of Geoscience and Mineral Resources, 124, Gwahak-ro Yuseong-gu, Daejeon 34132, Korea; leesaro@kigam.re.kr

\* Correspondence: wskee@kigam.re.kr

**Abstract:** The Jangsu-gun area in the central Southwestern South Korea consists of a well-preserved Middle Paleoproterozoic gneissic basement, as well as the Late Triassic and Early Jurassic granitic rocks. Here, we present the detailed zircon U-Pb age data and whole-rock chemical compositions, including radioactive elements (e.g., U and Th) and activity concentrations of <sup>226</sup>Ra, <sup>232</sup>Th and <sup>40</sup>K for the Middle Paleoproterozoic gneisses, and Late Triassic and Early Jurassic granitic rocks of the Jangsu-gun area. The Middle Paleoproterozoic gneissic basement, and the Late Triassic and Early Jurassic granitic rocks have ages of ca. 1988 Ma and 1824 Ma, 230 Ma and 187–189 Ma, respectively. Geochemically, the Middle Paleoproterozoic orthogneiss, Late Triassic granites and Early Jurassic granitic rocks show typical arc-related metaluminous to weakly peraluminous fractionated granite features with ASI (aluminum saturation index) values of 0.92 to 1.40. The mean values of U (ppm) and Th (ppm) of the Middle Paleoproterozoic orthogneisses (6.4 and 20.5, respectively), Late Triassic granites (1.5 and 10.9), and Early Jurassic granites (3.5 and 16.5) were similar to those (5 and 15) of the granitic rocks in the Earth's crust. The mean <sup>226</sup>Ra (Bq/kg), <sup>232</sup>Th (Bq/kg), and <sup>40</sup>K (Bq/kg) activity concentrations and radioactivity concentration index (RCI) are 62, 71, 1,214 and 0.96 for the Middle Paleoproterozoic orthogneisses; 16, 39, 1,614 and 0.78 for the Late Triassic granites; and 56, 70, 1031 and 0.88 for the Early Jurassic granitic rocks, respectively. The U, Th, <sup>226</sup>Ra, <sup>232</sup>Th, <sup>40</sup>K, and RCI of the Middle Paleoproterozoic biotite paragneisses are similar to those of the Middle Paleoproterozoic orthogneisses. The trend of <sup>226</sup>Ra, <sup>232</sup>Th, and <sup>40</sup>K activity concentrations, and the composition of U and Th from the Precambrian and Mesozoic rocks in the Jangsu-gun area indicates that monazite is the main accessory mineral controlling the concentration of natural radioactivity. Based on a detailed examination of the natural radioactivity in the rocks of the Jangsu-gun area, the Middle Paleoproterozoic orthogneisses and paragneisses, and Late Triassic and Early Jurassic granitic rocks show average high mean RCI values of 0.88–0.96, such that 32% of the rocks exceeded the recommended value of one in the guidelines for the RCI in South Korea. Especially, the RCI is closely related to the radon levels in the rocks. As a result, the Jangsu-gun area in South Korea is a relatively high radiological risk area, which exhibits higher indoor radon levels in the residences, compared with residences in the other areas in South Korea.

**Keywords:** Middle Paleoproterozoic; Late Triassic; Early Jurassic; granitic rock; central Southwestern South Korea; natural radioactivity



**Citation:** Kim, S.W.; Kee, W.-S.; Lee, S.; Lee, B.C.; Byun, U.H. Tracking and Evaluating the Concentrations of Natural Radioactivity According to Chemical Composition in the Precambrian and Mesozoic Granitic Rocks in the Jangsu-gun Area, Central Southwestern South Korea. *Minerals* **2021**, *11*, 684. <https://doi.org/10.3390/min11070684>

Academic Editor: Jean-Michel Lafon

Received: 25 April 2021

Accepted: 22 June 2021

Published: 25 June 2021

**Publisher's Note:** MDPI stays neutral with regard to jurisdictional claims in published maps and institutional affiliations.



**Copyright:** © 2021 by the authors. Licensee MDPI, Basel, Switzerland. This article is an open access article distributed under the terms and conditions of the Creative Commons Attribution (CC BY) license (<https://creativecommons.org/licenses/by/4.0/>).

## 1. Introduction

All minerals and raw materials in the rocks present on Earth commonly contain natural radioactive elements with radionuclides, but natural radioactivity exposures to

humans are substantially lower than the normal background levels in human activity; thus, there are no concerns regarding protection from radiation [1]. However, the natural radioactivity in some rocks can also cause high radiation exposure [1–7]. These rocks have been referred to as naturally occurring radioactive materials (NORMs). Among the NORMs, radionuclides of the  $^{238}\text{U}$  and  $^{232}\text{Th}$  decay series, and  $^{40}\text{K}$ , which potentially occur in the environment, are of the greatest interest. In addition, various social problems have arisen because of long-lived radioactive elements (e.g., uranium [U], thorium [Th] and potassium [K]) and their decay products (e.g., radium [Ra] and radon [Rn]) in household goods and construction materials. In South Korea, NORMs, such as U and Rn in soil or groundwater, have been investigated by the government for more than 20 years, and their origins have been closely connected with geological factors, such as rock chemical composition, deformation characteristics, and others [2–7].

In general, South Korea, in the southeastern part of the Asian continent (Figure 1A,B), is likely to have been located near a boundary of the continental plates during the Precambrian to Phanerozoic, creating an environment in which various rocks (igneous rock, metamorphic rock, and sedimentary rock) could form easily and be disrupted by igneous activities [6,8–15]. The Precambrian to Phanerozoic granitic rocks generated by this igneous activity occupy more than 40% of the land area in South Korea (Figure 1C) [11]. Consistent with NORMs, U and Th are enriched from the mantle to the lower continental crust and upper continental crust. Among the igneous rocks in the continental crust, U and Th are more enriched in the granitic rocks. This enrichment is caused by the processes of partial melting and fractional crystallization pertaining to granitic magma, which concentrate U and Th in the liquid phase and then into more silica-rich granitic rocks [5,16–19].

In South Korea, the granitic rocks comprise more than 90% of the domestic stone resources. Recently, natural rocks, in addition to building materials, have been presumed to affect overall radioactivity. Therefore, in South Korea, a standard guideline for reducing and managing radon in building materials has been applied since June of 2020, by a group of government ministries (Ministry of Environment, Ministry of Land, Infrastructure and Transport, and Nuclear Safety Committee) [20]. The essence of this guideline is to control radon contamination from building materials, by introducing a standard value according to the ‘radiation concentration index’, which is based on the radiological protection principles pertaining to the natural radioactivity of building materials, established by the European Union [21]. The target of management is natural stone-based materials that used as interior materials for buildings and apartment houses. The radioactivity concentration index is the ratio of the measured value to the combined radioactivity reference values of radium ( $^{226}\text{Ra}$ ), thorium ( $^{232}\text{Th}$ ), and potassium ( $^{40}\text{K}$ ), which are natural radioactive nuclides included in building materials. When the three ratios are summed, the value is one or less. The recommended standards for  $^{226}\text{Ra}$ ,  $^{232}\text{Th}$ , and  $^{40}\text{K}$ , which are natural radionuclides, are 300 Bq/kg for radium, 200 Bq/kg for thorium, and 3000 Bq/kg for potassium [20].

Recently, the Jangsu-gun area in central Southwestern South Korea has higher indoor radon levels in residential areas compared with other areas of South Korea. To understand natural radioactivity from the granitic rocks in the Jangsu-gun area, we report the concentrations of radioactive elements, such as U, Th, and K, with the activity concentrations of  $^{226}\text{Ra}$ ,  $^{232}\text{Th}$  and  $^{40}\text{K}$  for different Middle Paleoproterozoic, Late Triassic and Early Jurassic granitic rock samples from the Jangsu-gun area. We also report the U-Pb zircon age and geochemical data of the Middle Paleoproterozoic, Late Triassic and Early Jurassic granitic rocks, to clarify the relationships between the concentration trends of natural radioactivity and rock chemical composition.

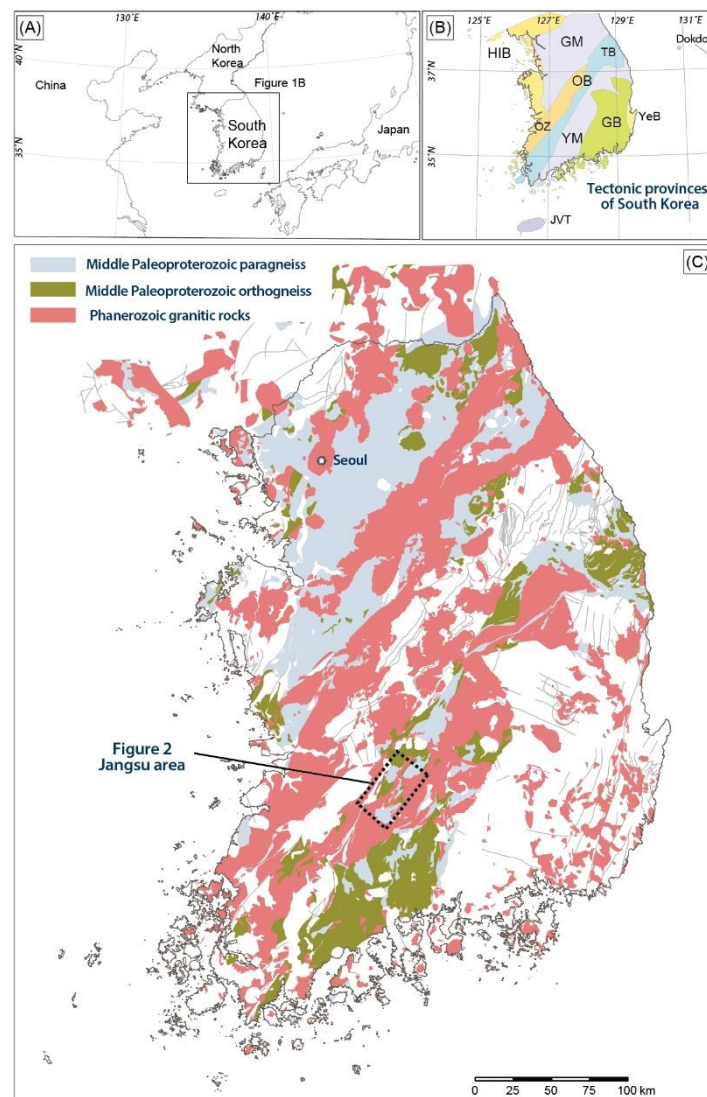


**Figure 1.** (A) Location map in the East Asian countries including South Korea, (B) tectonic map of South Korea, and (C) geological map of South Korea showing the distribution of the Middle Paleoproterozoic gneisses and Phanerozoic granitic rocks. HIB, Hongseong–Imjingang belt; GM, Gyeonggi massif; OB, Okcheon belt; YM, Yeongnam massif; GB, Gyeongsang basin; YeB, Yeonil basin; JVT, Jeju volcanic terrain.

## 2. Geological Setting

South Korea is located at the margin of the East Asian continent (Figure 1A). The tectonic provinces of South Korea largely consist of Precambrian (mainly Middle Paleoproterozoic) basement rocks, such as those of the Gyeonggi and Yeongnam massifs. The Precambrian basement rocks are separated by two narrow supracrustal units (the Hongseong–Imjingang and Okcheon belts). These provinces also include the Cretaceous Gyeongsang basin, Cenozoic Yeonil basin, and Jeju volcanic terrain, which formed after East Asian continent–continent collision during the Mesozoic (Figure 1B).

The study area is located in the Jangsu-gun area of central Southwestern South Korea; it is distributed within  $35^{\circ}28'$  to  $35^{\circ}49'$  N latitude and  $127^{\circ}22'$  to  $127^{\circ}42'$  E longitude, and has a total area of approximately  $533.43 \text{ km}^2$ . It is geologically located in the central-western area of the Precambrian Yeongnam massif. In the Jangsu-gun area, there is a wide distribution of the Middle Paleoproterozoic (2.02–1.96 Ga) basement gneisses, with minor gneisses of ca. 1.82 Ga (Figure 2) [14]. The Middle Paleoproterozoic gneisses are mainly intruded by the Late Triassic (ca. 230 Ma) and the Early Jurassic (187–180 Ma) granitic

rocks (Figure 2) [6,8–10,13,15,22–24]. The Middle Paleoproterozoic gneisses consist mainly of paragneisses (biotite paragneiss) and orthogneisses (granite orthogneiss, leucogranite orthogneiss, and porphyritic orthogneiss), with metasedimentary rocks (schist) and minor pegmatitic dikes and amphibolites (Figure 3A–F). The Middle Paleoproterozoic paragneisses also include granite orthogneiss, and minor pegmatitic dikes and amphibolites. The Middle Paleoproterozoic orthogneisses have well-developed gneissosity, with a K-feldspar megacryst- or augen-bearing banded magmatic structure. They include mainly quartz, plagioclase, biotite, and K-feldspar (microcline, and orthoclase), with or without hornblende and garnet. The Late Triassic granitic rocks are mainly porphyritic biotite granite, with K-feldspar megacrysts (Figure 3G,H). The Early Jurassic granitic rocks are mainly composed of hornblende-biotite granite, biotite granite, and two-mica granite with minor diorite and gabbro (Figure 3I–L). The Late Triassic porphyritic biotite and the Early Jurassic biotite, hornblende-biotite, and two-mica granites commonly include K-feldspar, plagioclase, quartz and biotite. However, the Early Jurassic hornblende-biotite and two-mica granite are characterized by the occurrence of hornblende and muscovite, respectively.

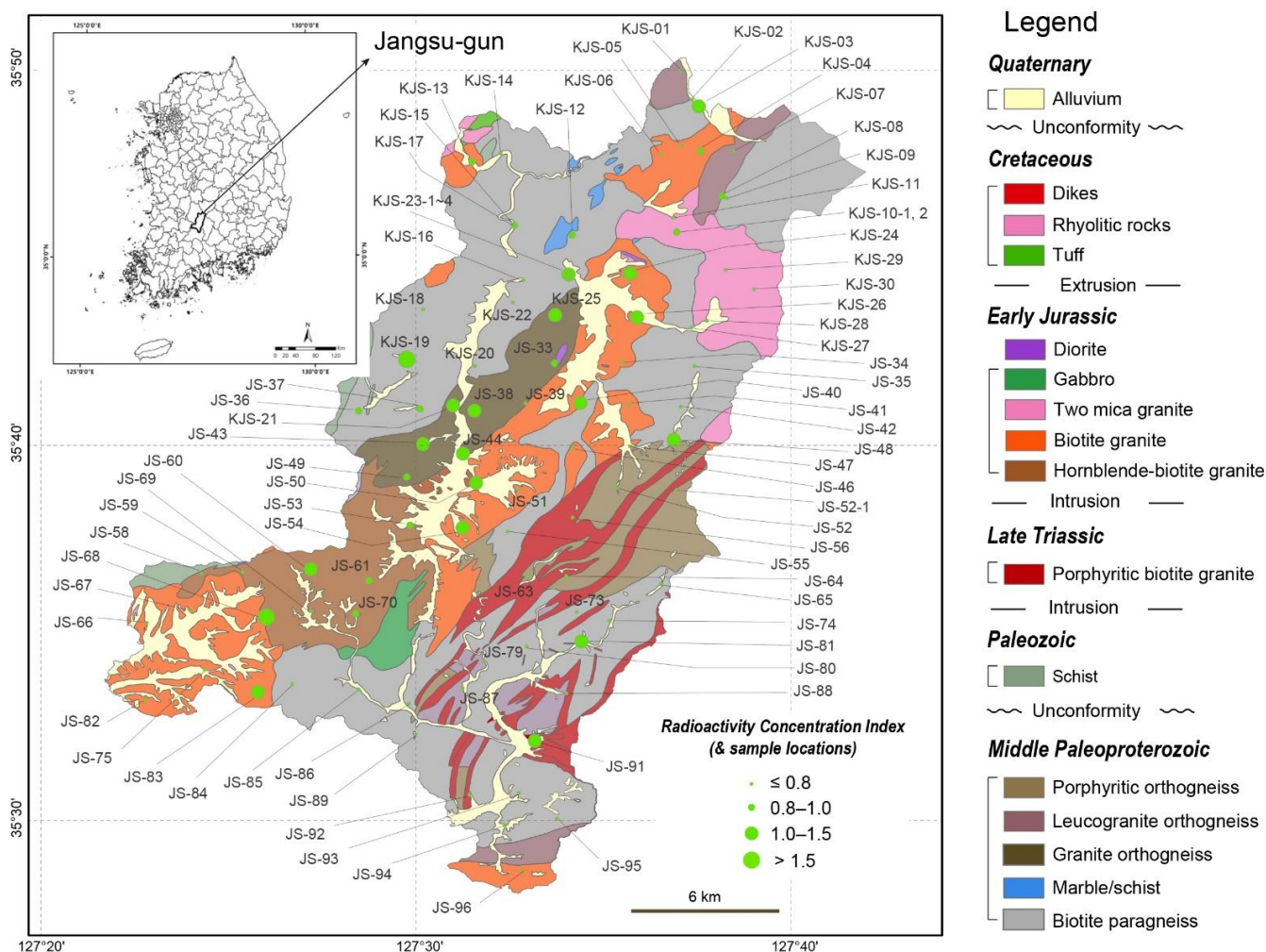


**Figure 2.** Sketch geologic maps of the Jangsu-gun area from the Southwestern Yeongnam massif, South Korea, showing the locations of samples analyzed in the present study.



**Figure 3.** Outcrop photographs showing (A,B) Middle Paleoproterozoic granite orthogneiss with magmatic flow structure, (C) Middle Paleoproterozoic leucogranite orthogneiss, (D) Middle Paleoproterozoic K-feldspar megacryst-bearing porphyritic orthogneiss, (E,F) Middle Paleoproterozoic banded biotite paragneiss having alternation of biotite paragneiss and granite orthogneiss, (G,H) Late Triassic biotite granite with textures commonly characterized by K-feldspar megacrysts, (I,J) Early Jurassic porphyritic biotite granite, (K) hornblende-biotite granite with or without K-feldspar megacrysts, and (L) Early Jurassic two-mica granite in the Jangsu-gun area.

### 3. Analytical Methods

Zircon Pb-Th-U isotopes were analyzed using a Nu Plasma II multi-collector inductively coupled plasma mass spectrometer (LA-MC-ICPMS), equipped with a New Wave Research 193-nm ArF excimer laser ablation system, at the Korea Basic Science Institute (KBSI). For some samples, U-Pb dating was also performed using a sensitive high-resolution ion microprobe (SHRIMP-IIe/MC) at the KBSI. Zircon grains were hand-picked from heavy mineral concentrates and mounted in epoxy. Before analysis, the grains were photographed under an optical microscope, and their internal zoning was imaged by cathodoluminescence (CL) using a JEOL 6610LV scanning electron microscope at KBSI (Figure 4). The conditions and data acquisition procedures were similar to those described by Kim et al. [15]. All ages were calculated with  $2\sigma$  error, and data reduction was conducted using Iolite 2.5 [25,26], SQUID 2.50 and Isoplot 3.71 [27,28]. The U-Pb results are listed in Table S1, and are illustrated on concordia plots in Figure 5.

Seventy-seven whole-rock samples of the Middle Paleoproterozoic orthogneisses and paragneisses, and Mesozoic granitic rocks were analyzed for major, trace, and rare earth element (REE) abundances, using inductively coupled plasma atomic emission spectrometry (ICP-AES) (ENVIRO II; Thermo Jarrel-Ash) and inductively coupled plasma mass spectrometry (ICP-MS) (Optima 3000; Perkin-Elmer) at Activation Laboratories, Ltd. (Ancaster, ON, Canada) (Table S2). The analytical uncertainties ranged from 1% to 3%.

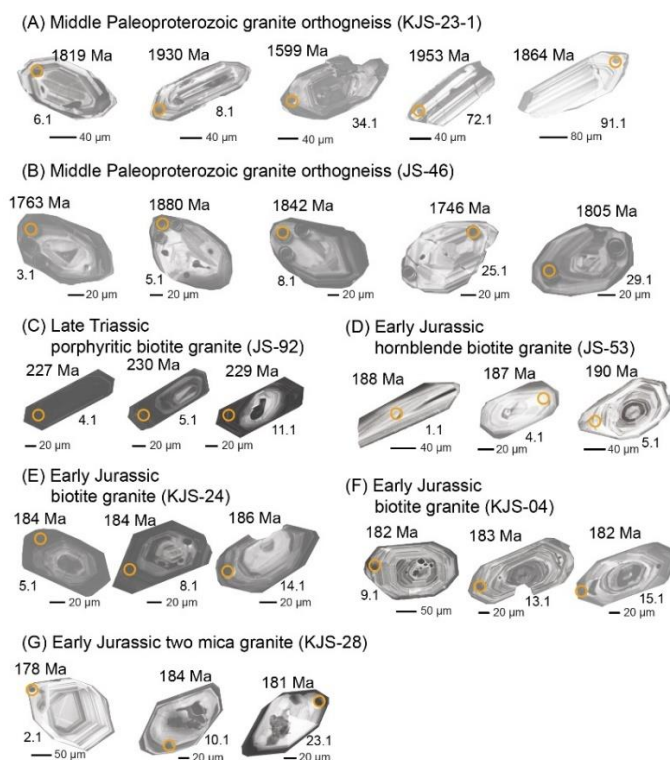


**Figure 4.** Scanning electron microscope (SEM) cathodoluminescence images of sectioned zircon grains from (A,B) Middle Paleoproterozoic granite orthogneisses, (C) Late Triassic porphyritic biotite granite, (D) Early Jurassic hornblende-biotite granite, (E,F) Early Jurassic biotite granites, and (G) Early Jurassic two mica granite in the Jangsu-gun area.

Precise determination of the activity of naturally occurring radionuclides ( $^{226}\text{Ra}$ ,  $^{232}\text{Th}$  and  $^{40}\text{K}$ ) was performed on seventy-seven whole-rock samples from the Jangsu-gun area, and the radioactivity concentration index was calculated. Most of the nuclide analyses were performed using a p-type high-purity germanium radiation detector (HPGe radiation detector) at the Hanil Nuclear Power Co., Ltd. A multichannel spectrum analyzer (BSI Hybrid, Latvia) was used for the measurement. The detector was calibrated through self-absorption correction, according to the energy and efficiency calibration density of the detector, using a geometrical standard source identical to the source used for the analysis sample. Each analysis sample was subjected to sample pretreatment processes, such as grinding, sieving, drying, mixing, and filling, using an aluminum mixing container; the amount of the sealed sample was generally 300 g. In particular, the sample was sealed and stored with consideration of the sample's radial equilibrium time. The  $^{226}\text{Ra}$  in the sample was measured after sealing and storing for more than three weeks, to prevent  $^{222}\text{Rn}$  from escaping out of the measuring container. For  $^{232}\text{Th}$ ,  $^{228}\text{Ac}$ , a progeny of Th, was measured immediately after sealing;  $^{40}\text{K}$  was also measured at that time. However, because it is inefficient to perform several measurements per sample, the three nuclides were measured concurrently using the p-type high-purity germanium (HPGe) radiation detector on the radiation-equilibrated sample, after it had been sealed for 25 days. The  $^{226}\text{Ra}$ ,  $^{232}\text{Th}$ , and  $^{40}\text{K}$  radioactivity concentrations obtained for each of the measured samples, together with their corresponding total uncertainties, are summarized in Table S3. Importantly, no radionuclides other than naturally occurring radionuclides were detected in the samples, and the small contribution of the environmental  $\gamma$ -ray background at the laboratory site was subtracted from the spectra of the measured samples.

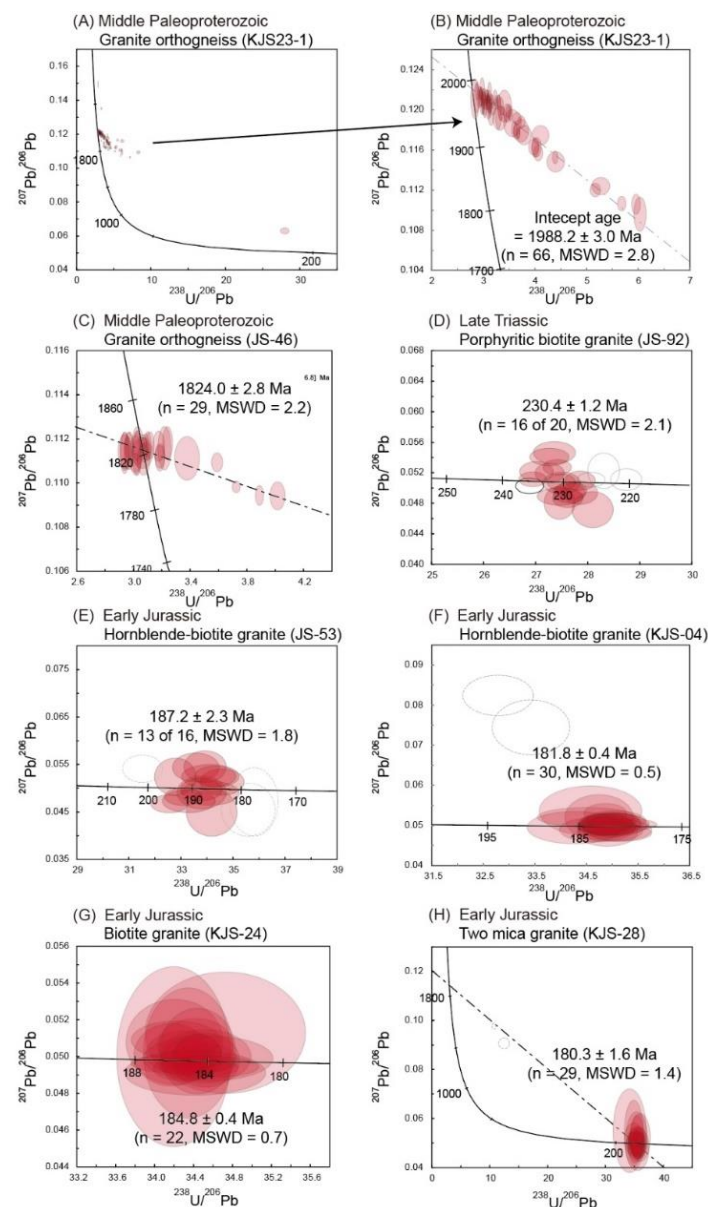


**Figure 5.** Tera–Wasserburg concordia plots of LA-MC-ICPMS and SHRIMP U–Pb isotopic analyses of zircons from the Middle Paleoproterozoic granite orthogneisses, Late Triassic and Early Jurassic granites in the Jangsun-gun area. KJS-23-1 Middle Paleoproterozoic granite orthogneiss (A,B), JS-46 Middle Paleoproterozoic granite orthogneiss (C), JS-92 Late Triassic biotite granite (D), JS-53 and KJS-04 Early Jurassic hornblende-biotite granites (E,F), KJS-24 Early Jurassic biotite granite (G), and KJS-28 Early Jurassic two-mica granite (H).

## 4. Results

### 4.1. U–Pb Geochronology

Granite orthogneisses (KJS23-1 and JS-46) from the Middle Paleoproterozoic gneissic rocks, one K-feldspar megacryst-bearing porphyritic biotite granite (JS-92) from the Late Triassic granite, two hornblende-biotite granite (JS-53 and KJS-04), one biotite porphyritic granite (KJS-24), and one two-mica granite (KJS-28) from the Early Jurassic granite in the Jangsu-gun area were selected for dating (Figure 2). Zircons commonly had euhedral shapes up to 50–350  $\mu\text{m}$  in diameter, with aspect ratios ranging from 1 to 4. All the grains had strong oscillatory growth zoning, which is typical of magmatic origin (Figure 4).

Granite orthogneisses with biotite paragneiss are regionally exposed in the Jangsu-gun area. Zircons from the granite orthogneisses in the biotite gneiss give dispersed ages

along the discordance line, which projected to a Middle Paleoproterozoic upper concordia intersection (Figure 5A,B). The precise estimate of the upper intersection age is obtained if all of the data are combined in a single regression, yielding  $1988.2 \pm 3.0$  Ma ( $n = 66$  of 100, MSWD = 2.8). On the other hand, zircons from small stock-type granite orthogneiss in granite orthogneiss and biotite paragneiss show younger Middle Paleoproterozoic age, giving an upper intercept  $^{207}\text{Pb}/^{206}\text{Pb}$  age of  $1824.0 \pm 2.8$  Ma ( $n = 29$ , MSWD = 2.2) (Figure 5C). Late Triassic granite plutons are exposed as a dike type in the southern part of the Jangsu-gun area. Zircons from the Late Triassic granite sample (KJS-24) give a weighted mean  $^{206}\text{Pb}/^{238}\text{U}$  age of  $230.4 \pm 1.2$  Ma (Figure 5D). Early Jurassic granite plutons are mainly exposed in the central part of the Jangsu-gun area. Zircons from the hornblende-biotite granite samples (JS-53 and KJS-04) give weighted mean  $^{206}\text{Pb}/^{238}\text{U}$  ages of  $187.2 \pm 2.3$  Ma and  $181.8 \pm 0.4$  Ma, respectively (Figure 5E,F). Zircons from the biotite granite sample (KJS-24) give a weighted mean  $^{206}\text{Pb}/^{238}\text{U}$  age of  $184.8 \pm 0.4$  Ma (Figure 5G). Most of the analyzed zircons with oscillatory zoning from two-mica granite give a weighted mean  $^{206}\text{Pb}/^{238}\text{U}$  age of  $180.3 \pm 1.6$  Ma (Figure 5H).

#### 4.2. Geochemistry

The Middle Paleoproterozoic granite orthogneisses, and Early Jurassic granitic rocks from the Jangsu-gun area were mainly analyzed to determine their geochemical signatures (Table S2). The Middle Paleoproterozoic biotite paragneisses and Late Triassic granites were also analyzed to interpret geochemical characteristics in the Jangsu-gun area. On the  $\text{SiO}_2$  versus  $\text{Na}_2\text{O} + \text{K}_2\text{O}$  diagram, with fields defined by [29] (Figure 6), the ca. 1.99 Ga Middle Paleoproterozoic samples mainly plotted in the diorite, quartz monzonite, quartz diorite and granite fields. The ca. 1.82 Ga Middle Paleoproterozoic orthogneiss samples are plotted in the quartz diorite and granite fields. The Late Triassic porphyritic granite and Early Jurassic biotite granite samples are also plotted in the quartz diorite and granite fields. The Early Jurassic hornblende-biotite granite samples are mainly plotted in quartz diorite, and the Early Jurassic two-mica granite samples are plotted in the granite field.

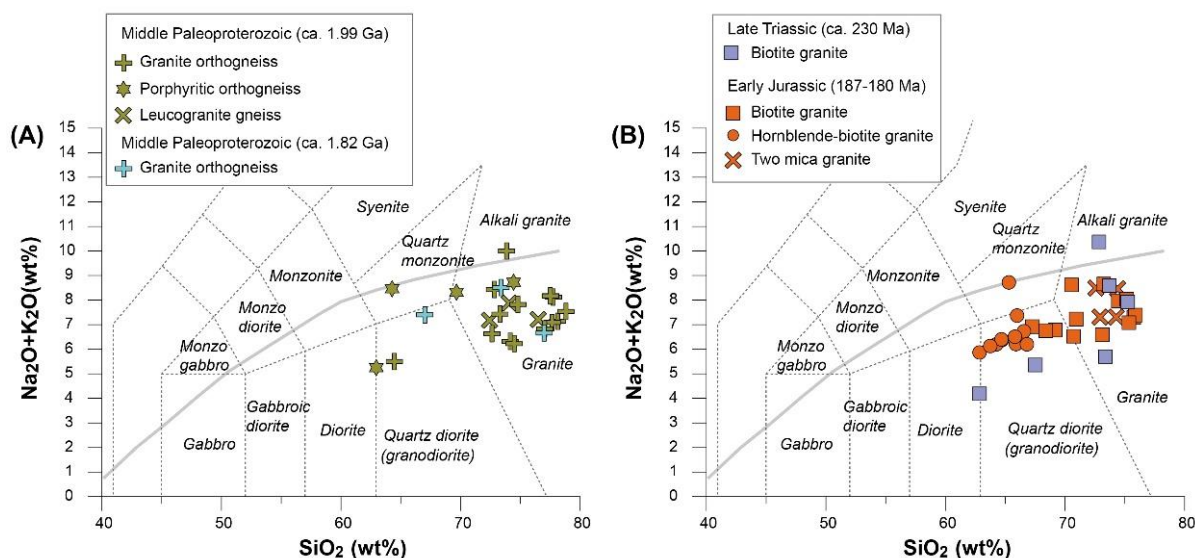


**Figure 6.**  $\text{SiO}_2$  wt.% versus  $\text{Na}_2\text{O} + \text{K}_2\text{O}$  wt.% diagram for the Middle Paleoproterozoic orthogneisses (A), and Late Triassic granite and Early Jurassic granitic rocks (B) in the Jangsu-gun area.

The major element abundances plotted against  $\text{SiO}_2$  of the orthogneisses (leucogranite orthogneiss, porphyritic orthogneiss, and granite orthogneiss) with biotite paragneisses, Late Triassic porphyritic granite and Early Jurassic granitic rocks show negative correlations with  $\text{Al}_2\text{O}_3$ ,  $\text{Fe}_2\text{O}_3^*$ ,  $\text{MgO}$ ,  $\text{CaO}$ ,  $\text{P}_2\text{O}_5$  and  $\text{TiO}_2$ ; they show no correlations with  $\text{K}_2\text{O}$  or  $\text{Na}_2\text{O}$  (Figure 7). The Middle Paleoproterozoic orthogneisses have most weakly

peraluminous in an aluminum saturation index (ASI) defined by Shand [30], which ranged from 0.95 to 1.20 (Figure 8). The Late Triassic porphyritic biotite granite and Early Jurassic biotite, and two-mica granites are also weakly peraluminous (ASI = 1.00 to 1.39), with the exception of one low ASI (0.7). The Early Jurassic hornblende-biotite granites ranged from metaluminous to weakly peraluminous (ASI = 0.93 to 1.13).

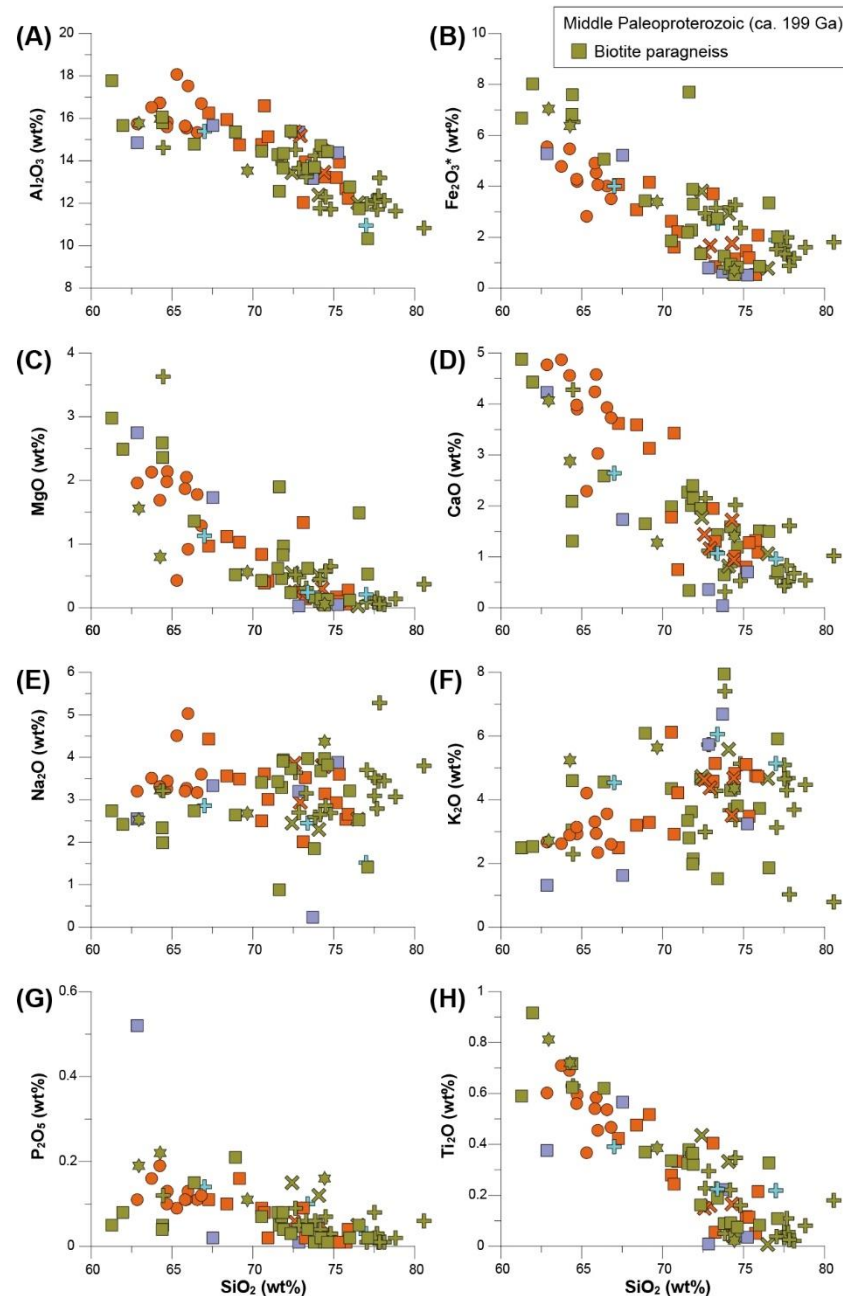


**Figure 7.** Plots of major elements (A)  $\text{Al}_2\text{O}_3$ , (B)  $\text{Fe}_2\text{O}_3^*$ , (C)  $\text{MgO}$ , (D)  $\text{CaO}$ , (E)  $\text{Na}_2\text{O}$ , (F)  $\text{K}_2\text{O}$ , (G)  $\text{P}_2\text{O}_5$ , and (H)  $\text{TiO}_2$  versus  $\text{SiO}_2$  for the Middle Paleoproterozoic gneisses, Late Triassic granite, and Early Jurassic granitic rocks in the Jangsu-gun area. Symbols are as in Figure 6.

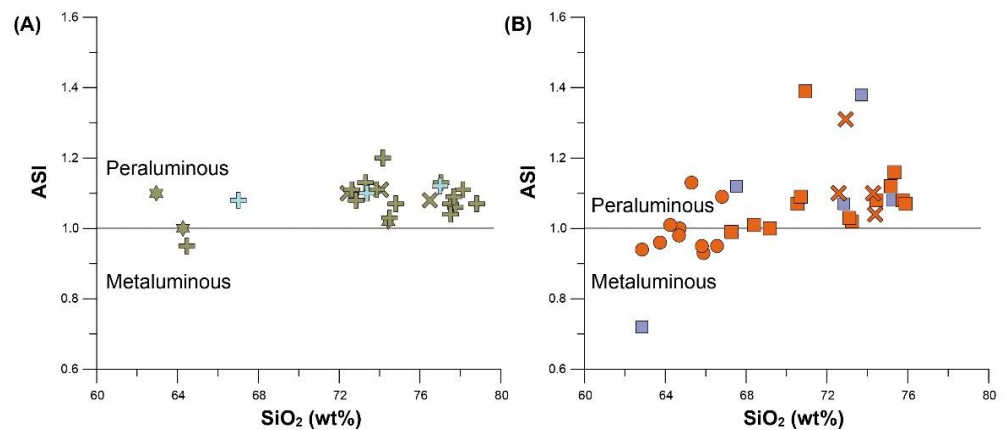


**Figure 8.**  $\text{SiO}_2$  wt.% versus ASI diagram [30] for the Middle Paleoproterozoic orthogneisses (A), and Late Triassic granite and Early Jurassic granitic rocks (B) in the Jangsu-gun area. ASI:  $\text{Al}/(\text{Ca} - 1.67\text{P} + \text{Na} + \text{K})$ . Symbols are as in Figure 6.

The chondrite-normalized rare earth elements (REE) distribution patterns of the Middle Paleoproterozoic leucogranite orthogneiss, porphyritic orthogneiss, granite orthogneisses with biotite paragneisses, Late Triassic porphyritic granite and Early Jurassic biotite granite, hornblende-biotite granite and two-mica granite have commonly light REE enrichments (Figure 9). Most rock samples have moderately negative to strongly positive Eu anomalies (0.4–2.86), but many Middle Paleoproterozoic granite orthogneiss samples show strongly negative Eu anomalies (0.02–0.38). On the primitive mantle normalized diagrams (Figure 9), the Middle Paleoproterozoic and Early Jurassic rock samples from the Jangsu-gun area display large ion lithophile element (LILE) enrichment with Ta–Nb troughs, as well as P and Ti depletions. The Middle Paleoproterozoic samples also show Sr depletion, in comparison with the Late Triassic and Early Jurassic granite samples (Figure 9).

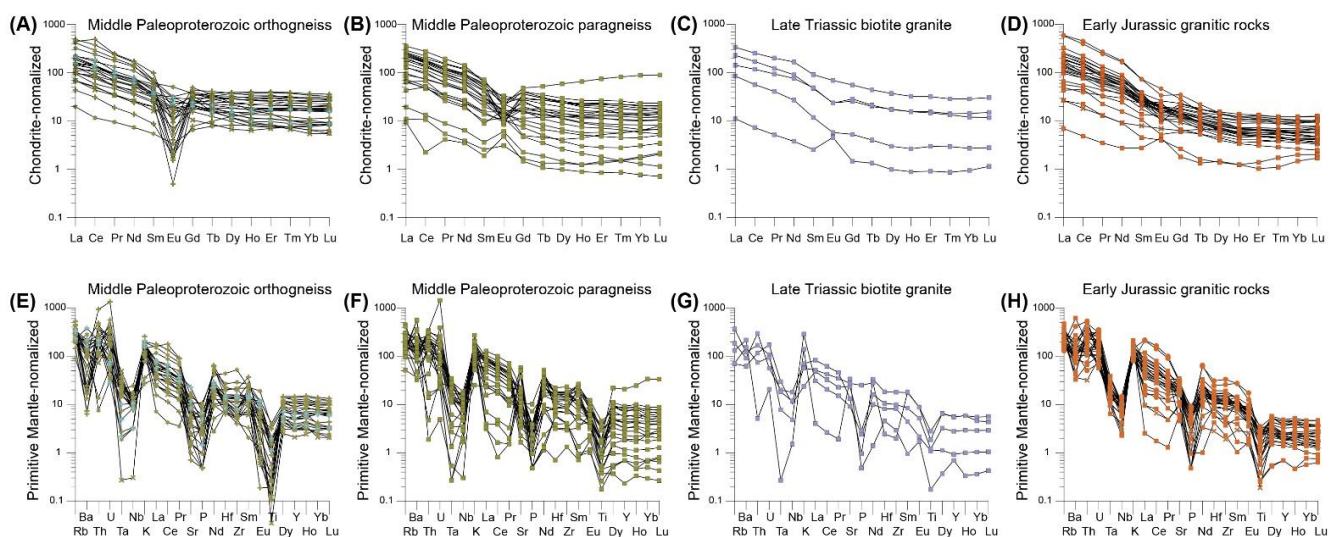


**Figure 9.** (A–D) Chondrite-normalized rare earth element (REE) patterns, and (E–H) primitive mantle-normalized trace element distribution diagrams [31] for the Middle Paleoproterozoic orthogneisses, biotite gneisses, Late Triassic granite and Early Jurassic granitic rocks in the Jangsu-gun area. Symbols are as in Figures 6 and 7.

### 4.3. Gamma Nuclide Analysis

The activity concentrations of  $^{226}\text{Ra}$ ,  $^{232}\text{Th}$  and  $^{40}\text{K}$  from the ca. 1.99 Ga orthogneisses in the Jangsu-gun area are 19–42, 46–67, and 1148–1621 Bq/kg for leucogranitic orthogneiss; 9–12, 3–86, and 929–1530 Bq/kg for porphyritic orthogneiss; and 21–241, 29–140, and 473–1857 Bq/kg for the granite orthogneiss, respectively. All the radiation concentration index (RCI) values are within the range of 0.48 to 1.98 (Figure 10A–C). Among the 21 samples, 10 samples showed a high RCI of 1.00 to 1.98 (Figure 10A–C). The concentrations of  $^{226}\text{Ra}$ ,  $^{232}\text{Th}$ , and  $^{40}\text{K}$  for the 2.02–1.96 Ga biotite gneisses with granite orthogneisses were 4–81, 4–94, and 421–1603 Bq/kg, respectively, and the RCI values are within an intermediate range of 0.39 to 1.02 (Figure 10D). Two of the 21 samples show a value higher than 1.00. In contrast, the concentrations of  $^{226}\text{Ra}$ ,  $^{232}\text{Th}$ , and  $^{40}\text{K}$  for the ca. 1.82 Ga small-stock-type granite orthogneiss in the Jangsu-gun area are 6–16, 42–61, and 1083–1604 Bq/kg, respectively; the RCI values are within the narrow range of 0.72 to 0.76 (Table S3).

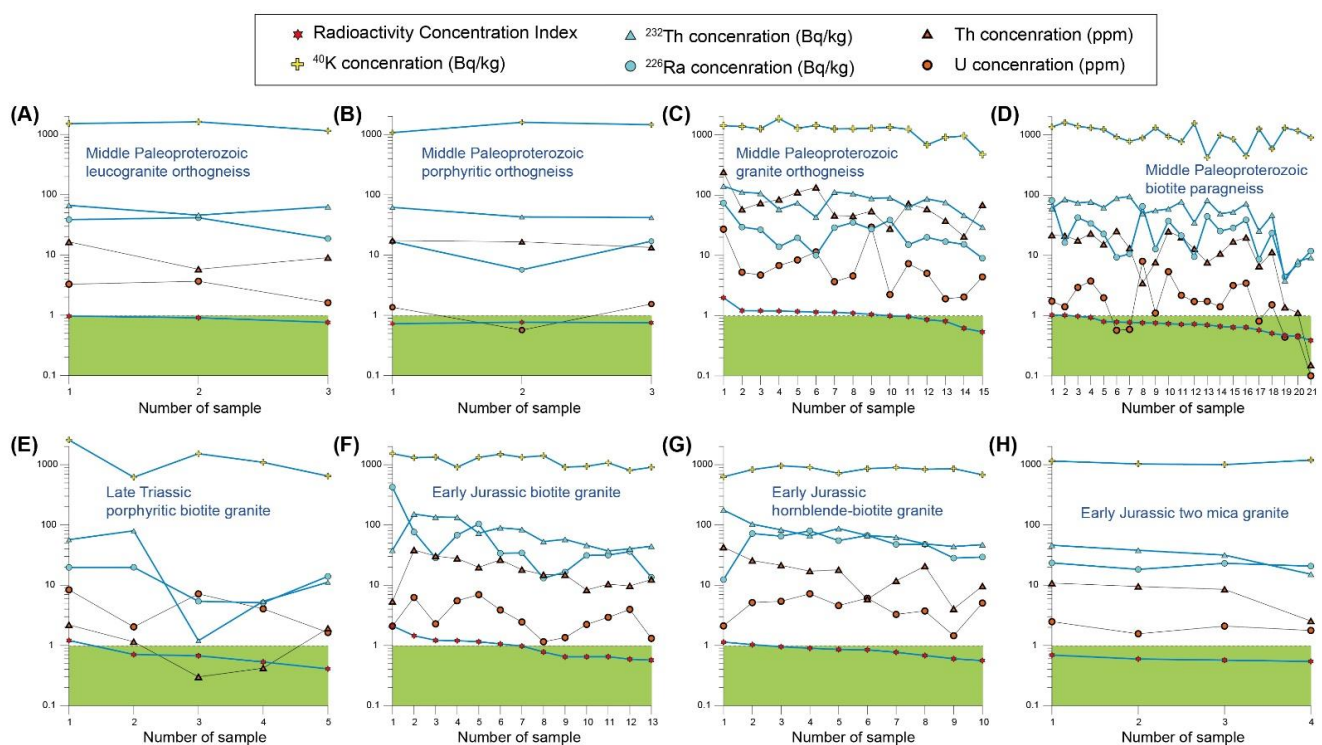


**Figure 10.** Plots of U and Th concentrations of geochemical analysis and the activity concentrations of  $^{226}\text{Ra}$ ,  $^{232}\text{Th}$ ,  $^{40}\text{K}$  and RCI values for (A–D) Middle Paleoproterozoic granite orthogneisses, (E) Late Triassic porphyritic biotite granite, (F) Early Jurassic biotite granite, (G) Early Jurassic hornblende biotite granite, and (H) Early Jurassic two mica granite in the Jangsu-gun area.

The concentrations of  $^{226}\text{Ra}$ ,  $^{232}\text{Th}$  and  $^{40}\text{K}$  for the Late Triassic (ca. 230 Ma) porphyritic biotite granite are 5 to 19, 1 to 80, and 625 to 2,570 Bq/kg, respectively, and the RCI values are within the intermediate range of 0.32 to 1.21 (Figure 10E). The concentrations of  $^{226}\text{Ra}$ ,  $^{232}\text{Th}$ , and  $^{40}\text{K}$  for the Early Jurassic (187–180 Ma) biotite granite are 13–422, 37–154, and 808–1,531 Bq/kg, respectively, and the RCI ranged from Middle to high values of 0.57 to 2.10 (Figure 10F). Six of the 13 samples have an RCI value higher than 1.00. The Early Jurassic (187–180 Ma) hornblende-biotite granite has concentrations, for  $^{226}\text{Ra}$ ,  $^{232}\text{Th}$  and  $^{40}\text{K}$ , of 12–76, 43–173, and 630–960 Bq/kg, respectively; the RCI has a wide range of 0.56 to 1.12 (Figure 10G). Two among the eleven samples show a high activity concentration index (1.02 and 1.12, respectively). The concentrations of  $^{226}\text{Ra}$ ,  $^{232}\text{Th}$ , and  $^{40}\text{K}$  of the Early Jurassic (187–180 Ma) two-mica granite are 18–23, 16–46, and 1002–1191 Bq/kg, respectively; the RCI had intermediate values of 0.54 to 0.69 (Figure 10H).

## 5. Discussion

### 5.1. Petrogeneses of the Middle Paleoproterozoic Orthogneiss, Late Triassic Granite and Early Jurassic Granitic Rocks of the Jangsu-gun Area

From the LA-MC-ICPMS and SHRIMP U-Pb zircon ages presented in this study, there is the possibility to characterize the Middle Paleoproterozoic (ca. 1.99 Ga and ca. 1.82 Ga) magmatic events, and Late Triassic (ca. 230 Ma) and Early Jurassic (187–180 Ma) magmatic events in the Jangsu-gun area (Figure 8).

The trace elements and REE geochemical characteristics of them are similar to those of subduction-related granitic rocks, with a subalkalic chemical trend. In the classification established by Pearce et al. [32], they occupy the volcanic arc granitoid field (Figure 11).

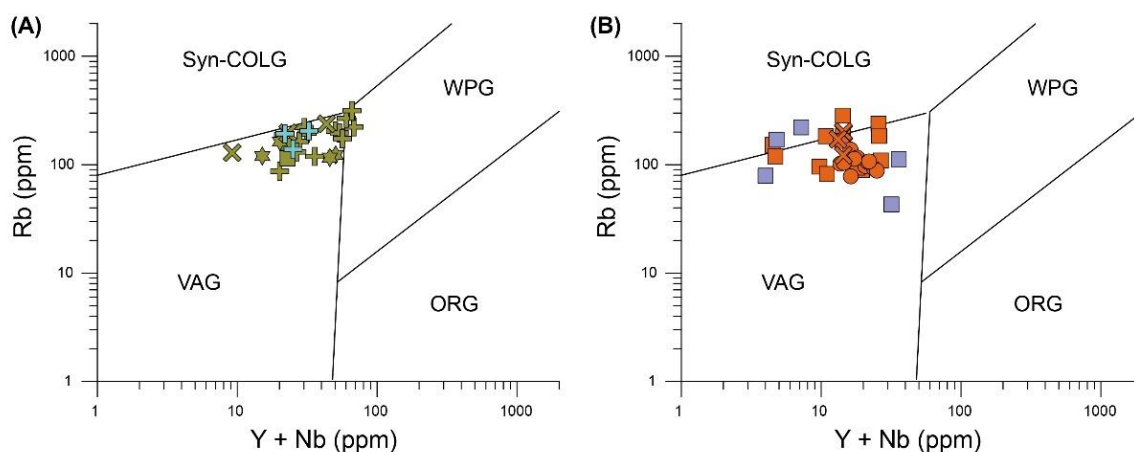


**Figure 11.** Rb versus (Y + Nb) tectonic discrimination diagram for (A) the Middle Paleoproterozoic orthogneisses, and (B) Late Triassic granite and Early Jurassic granitic rocks in the Jangsu-gun area. VAG, volcanic arc granites; ORG, ocean ridge granites; WPG, within-plate granites; syn-COLG, syn-collision granites. Symbols are as in Figure 6.

The ASI values of the Middle Paleoproterozoic orthogneisses (1.0 to 1.1, except for some samples with values 1.1 to 1.2) show the characteristics of weakly peraluminous granites. Moreover, in many parts of the Jangsu-gun area, biotite gneiss (i.e., metasedimentary rock) is widely distributed. The Late Triassic and Early Jurassic granitic rocks in the Jangsu-gun area showed metaluminous to weakly peraluminous granite characteristics, with an ASI of 0.9 to 1.1. In some rocks, the ASI values range from 1.1 to 1.4. An ASI value change of 0.9 to 1.4 in the Middle Paleoproterozoic orthogneisses, and Late Triassic and Early Jurassic granitic rocks in the Jangsu-gun area discriminates amphibole and pyroxene formation during magma crystallization, which increases the ASI value of the residual melt. This reveals the evolution process to peraluminous granites containing biotite and muscovite. Therefore, tracking the degree of fractional crystallization or partial melting of granitic rocks provides important information that is useful for explaining the petrogeneses of granitic rocks distributed in the Jangsu-gun area [33].

The degree of fractional crystallization in the peraluminous granitic rocks can be determined from the Nb/Ta ratio in the whole-rock chemistry (Figure 12) [34]. In general, a decrease in the Nb/Ta ratio in evolved melts suggests effects of both fractional crystallization and sub-solidus hydrothermal alteration. The extensively surveyed Middle Paleoproterozoic orthogneiss and Early Jurassic granitic rocks in the Jangsu-gun area show a degree of fractional crystallization of approximately 50%, with a maximum Nb/Ta of five. However, most of these rocks in the Jangsu-gun area do not show Nb/Ta values much lower than five, and therefore the role of sub-solidus hydrothermal alteration in their late stages of evolution is considered to be insufficient.

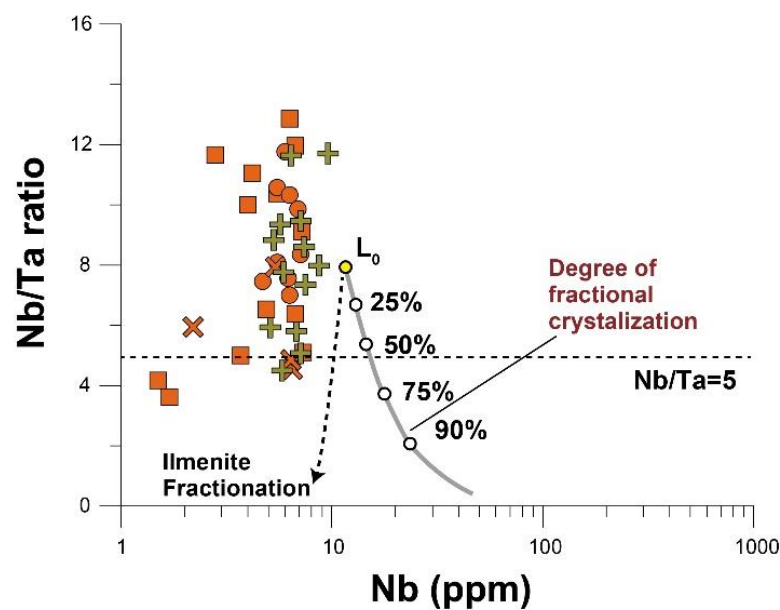


**Figure 12.** Nb versus Nb/Ta diagram for the Middle Paleoproterozoic orthogneisses and Early Jurassic granitic rocks in the Jangsu-gun area. Grey-colored curves represent model of evolution of Nb and Ta in liquid  $L_0$  ( $Nb = 12$  ppm,  $Ta = 1.5$  ppm,  $Nb/Ta = 8$ ) during fractionation of assemblage made of 10 wt.% biotite + 10 wt.% muscovite + 80 wt.% (quartz and feldspar). Numbers above curves indicate amount of fractional crystallization. Black dashed line represents same model during fractionation of assemblage composed of 10 wt.% biotite + 10 wt.% muscovite + 0.5 wt.% ilmenite + 79.5 wt.% (quartz and feldspar). Symbols are as in Figure 4.

Nevertheless, zircon Hf data of the Middle Paleoproterozoic (ca. 1.99 Ga) gneisses in the Jangsu-gun area have been suggested to reflect ancient crustal material that may have been extracted from the depleted mantle at ca. 3022–3670 Ma [14]. These subduction-related Middle Paleoproterozoic (ca. 1.99 Ga) gneisses occur widely along the northern margin of the Yeongnam massif [14]. The zircon Hf data of the Late Triassic (ca. 230 Ma) and Early Jurassic (187–180 Ma) granitic rocks in the Jangsu-gun area, together with the whole-rock Sr and Nd isotopic data [8–10], strongly reflect the mixing between primitive melts originated from the lithospheric mantle and the arc-related Middle Paleoproterozoic basement [13].

### 5.2. Tracking of NORMs from the Granitic Rocks in the Jangsu-gun Area

The natural radioactivity levels from the Middle Paleoproterozoic orthogneisses and paragneisses, and Late Triassic and Early Jurassic granitic samples in the Jangsu-gun area may be related to the occurrence characteristics of radioactivity-related accessory minerals (i.e., with high concentrations of radioactive elements), and feldspar in the intermediate to felsic rocks. The Middle Paleoproterozoic orthogneisses and paragneisses, and Late Triassic and Early Jurassic granitic samples in the Jangsu-gun area commonly include zircon, uraninite and monazite of the accessory minerals, and K-feldspar of the main minerals. The variations between  $^{226}\text{Ra}$ ,  $^{232}\text{Th}$ , and  $^{40}\text{K}$  activity concentrations, and U, Th and  $\text{K}_2\text{O}$  contents in the whole-rock chemistry from the Middle Paleoproterozoic orthogneisses, and Late Triassic and Early Jurassic granitic samples with continuously evolving smooth linear positive trends well support the presences of them (Figure 13). On variation diagrams in between  $^{226}\text{Ra}$ ,  $^{232}\text{Th}$ , and  $^{40}\text{K}$  activity concentrations and RCI (radiation concentration index) value from the Middle Paleoproterozoic orthogneiss and paragneiss, and Early Jurassic granitic samples (Figure 14), the RCI values of the peraluminous Early Jurassic granitic rocks show a good positive correlation with  $^{226}\text{Ra}$  and  $^{232}\text{Th}$  concentration. In contrast, the Middle Paleoproterozoic paragneisses show rough positive linear trends between  $^{226}\text{Ra}$ ,  $^{232}\text{Th}$ , and  $^{40}\text{K}$  activity concentrations, and U, Th and  $\text{K}_2\text{O}$  contents (Figure 13). They also

display a rough positive correlation between RCI values, and  $^{226}\text{Ra}$  and  $^{232}\text{Th}$  concentration (Figure 14). The metaluminous Early Jurassic hornblende-biotite granite samples show no correlation between  $^{40}\text{K}$  activity concentration and  $\text{K}_2\text{O}$  content, because they have an insufficient amount of K-feldspar in the rocks (Figure 13).

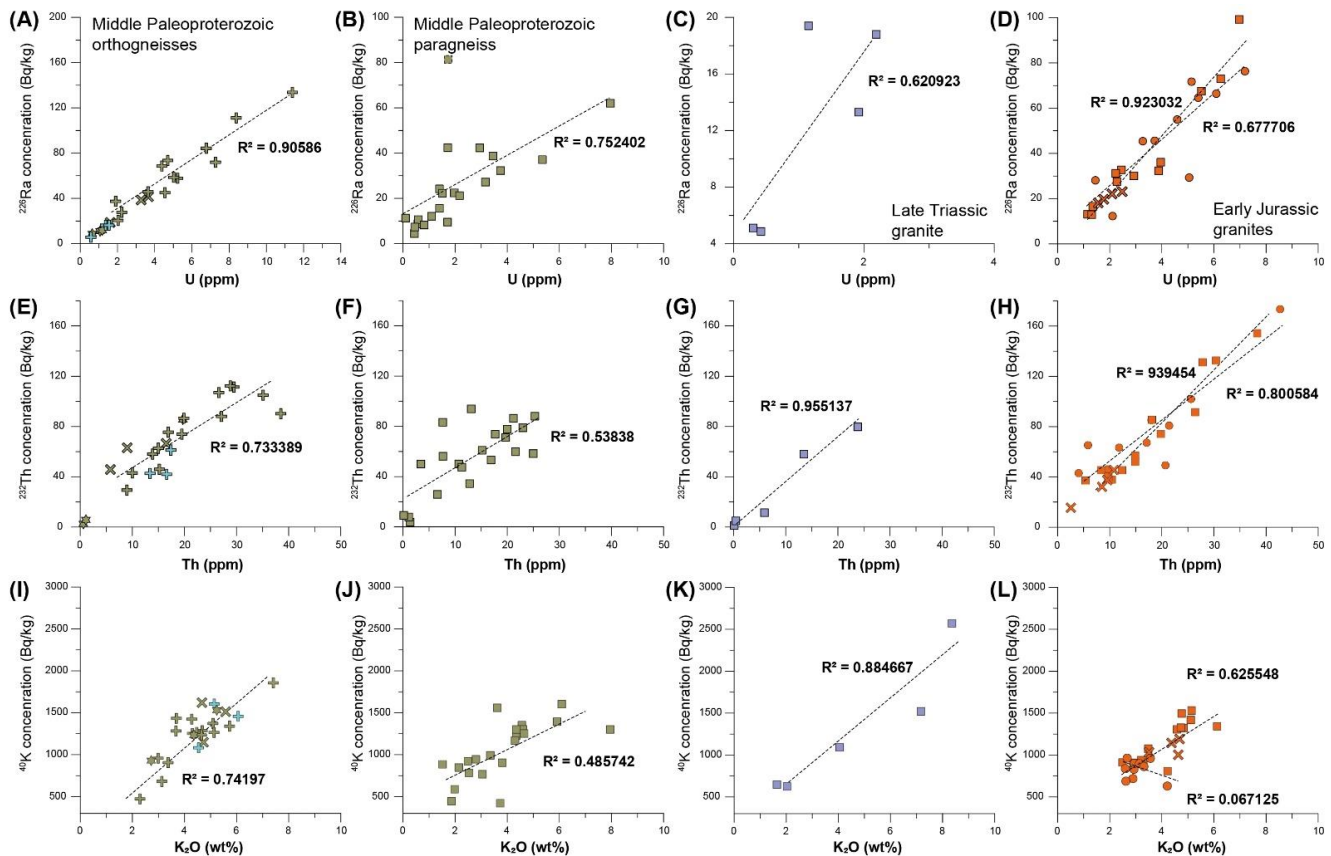


**Figure 13.**  $^{226}\text{Ra}$  versus U,  $^{232}\text{Th}$  versus Th, and  $^{40}\text{K}$  versus  $\text{K}_2\text{O}$  diagrams for the Middle Paleoproterozoic orthogneisses (A,E,I), Middle Paleoproterozoic paragneisses (B,F,J), Late Triassic granite (C,G,K), and Early Jurassic granites (D,H,L) in the Jangsu-gun area.  $R^2$  is value using linear regression for the number of analyzed samples in each rock unit. Symbols are as in Figures 6 and 7.

In the present study, the Middle Paleoproterozoic granite orthogneisses and paragneisses, and Early Jurassic biotite and hornblende-biotite granites, with many analyzed samples, are a good positive correlation between  $^{232}\text{Th}$  concentration and RCI values, compared with  $^{226}\text{Ra}$  and  $^{40}\text{K}$  (Figure 14). This reason can be assumed to be that monazite is the main accessory mineral controlling the concentrations of NORMs in Middle Paleoproterozoic and Early Jurassic rocks distributed in the Jangsu-gun area; although zircon, apatite, and titanite can generally be produced as accessory minerals containing U and Th in the rocks. Monazite exhibits strong compositional differences at a variety of scales in the granitic rocks [35]. In addition, monazite in peraluminous granites is reported to be of higher importance, of all the investigated elements, for the rock budget (e.g., U, Th and Y) in peraluminous granites than zircon, as an important carrier of Y and U [36].

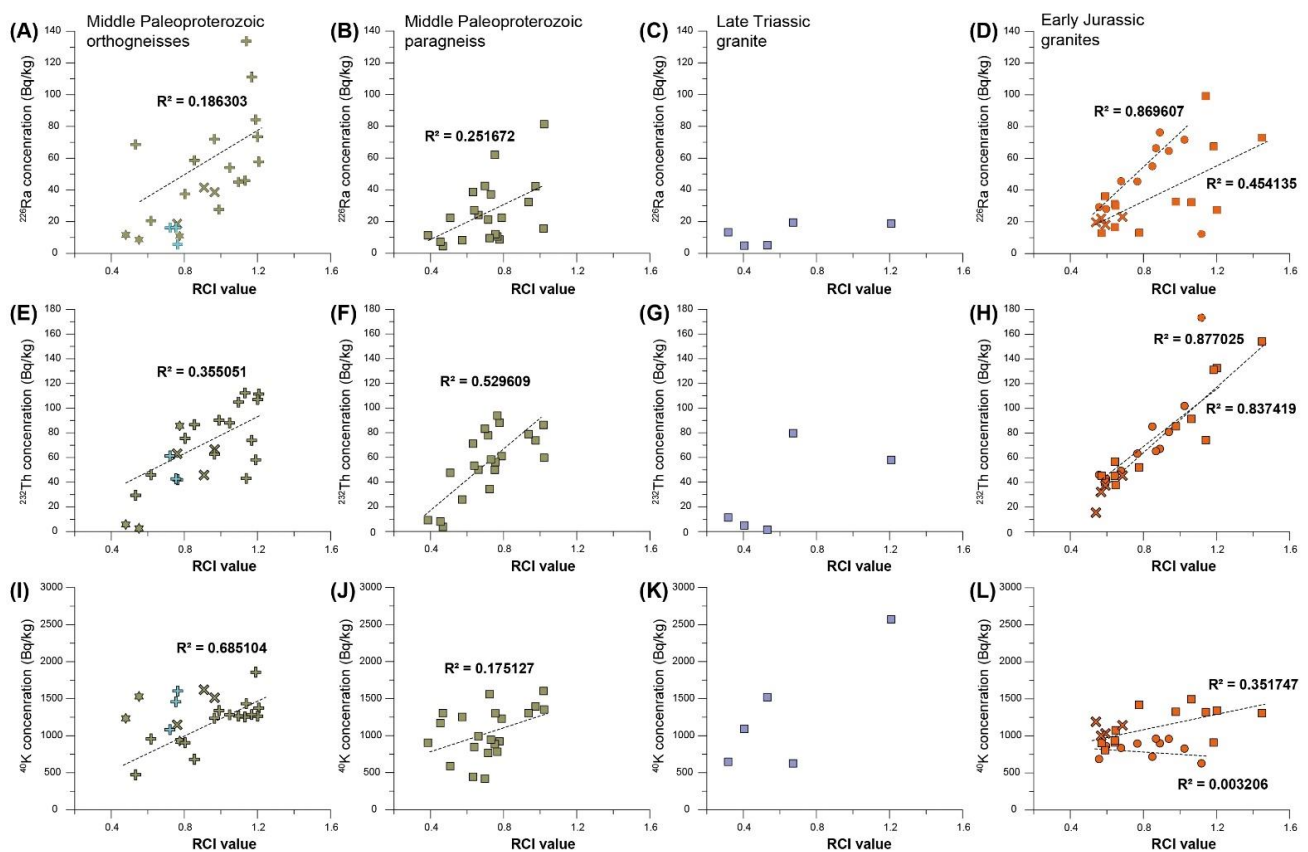


**Figure 14.** Plots of the concentrations of  $^{226}\text{Ra}$ ,  $^{232}\text{Th}$ ,  $^{40}\text{K}$ , and RCI values for the Middle Paleoproterozoic orthogneisses (A,E,I), Middle Paleoproterozoic paragneisses (B,F,J), Late Triassic granite (C,G,K), and Early Jurassic granites (D,H,L) in the Jangsu-gun area. RCI, radiation concentration index. Symbols are as in Figures 6 and 7.

The RCI values for the Middle Paleoproterozoic gneisses and the Early Jurassic granitic rocks in the Jangsu area indicate that 32% of the rocks exceed the RCI guideline value of one for natural stone construction materials in South Korea, and that 58% of the rocks have a high RCI value of 0.8 or more (Table S3). Recently, in a preliminary study of natural radioactivity levels of 72 samples of the representative Permian, Triassic, Jurassic and Cretaceous granitic rocks in South Korea, 29% of the rocks have been reported to have a high RCI value of 0.8 or more [6]. The  $^{226}\text{Ra}$ ,  $^{232}\text{Th}$ , and  $^{40}\text{K}$  activity concentrations with the high RCI values in the rocks are being reported, which can affect the lungs or organs of the human body within an enclosed indoor space [21]. The RCI value must be reported in the use of finishing materials for natural stone in South Korea's apartment houses, and the use of natural stone is beginning to be regulated [20]. Therefore, regional and systematic studies on  $^{226}\text{Ra}$ ,  $^{232}\text{Th}$ , and  $^{40}\text{K}$  activity concentrations, and the RCI value of various rocks in South Korea, are required.

## 6. Conclusions

The Middle Paleoproterozoic (ca. 1.99 Ga and ca. 1.82 Ga) gneisses form the basement in the Jangsu-gun area, while the Late Triassic (ca. 230 Ma) and Early Jurassic granitic rocks (187–180 Ma) mainly intrude the Middle Paleoproterozoic gneisses. The Middle Paleoproterozoic orthogneiss, and Late Triassic and Early Jurassic granitic rocks show arc-related granite features and have a weak to medium degree of fractional crystallization, from metaluminous to weakly peraluminous granite, with ASI values of 0.92 to 1.40. The Middle Paleoproterozoic orthogneisses and paragneisses, and Late Triassic and Early Jurassic granitic rocks commonly have high concentrations of natural radioactivity compared with the other gneiss and granitic rocks in South Korea. The trend of  $^{226}\text{Ra}$ ,  $^{232}\text{Th}$ , and  $^{40}\text{K}$

activity concentrations, and the composition of trace elements (e.g., U and Th) from the Middle Paleoproterozoic orthogneisses, and Late Triassic and Early Jurassic granitic rocks in the Jangsu-gun area, indicate that monazite is the main accessory mineral controlling the concentration of NORMs. Based on a detailed examination of the concentration changes in natural radioactivity in the granitic rocks of the Jangsu-gun area, 32% of the rocks exceed the recommended value of one of the guidelines for the RCI in South Korea. Therefore, the Jangsu-gun area presumably has a high concentration of NORMs, which results in higher indoor radon levels in residences, compared with residences in the parts of South Korea. Accordingly, careful tracking and management of natural radioactive substances from rocks is required in the Jangsu area of central Southwestern South Korea.

**Supplementary Materials:** The following are available online at <https://www.mdpi.com/article/10.3390/min11070684/s1>, Table S1: U-Pb zircon data of the Middle Paleoproterozoic, Late Triassic and Early Jurassic rocks in the Jangsu-gun areas in South Korea, Table S2: major and trace element analyses of the Middle Paleoproterozoic, Late Triassic and Early Jurassic rocks in the Jangsu-gun areas in South Korea, Table S3: natural radioactivity concentrations of  $^{226}\text{Ra}$  ( $^{238}\text{U}$ ),  $^{232}\text{Th}$  and  $^{40}\text{K}$  in the Middle Paleoproterozoic, Late Triassic and Early Jurassic rocks in the Jangsu-gun areas in South Korea.

**Author Contributions:** Data curation, S.W.K., W.-S.K. and S.L.; formal analysis, S.W.K., W.-S.K., B.C.L. and U.H.B.; funding acquisition, S.W.K.; investigation, S.W.K., W.-S.K., B.C.L. and U.H.B.; methodology, S.W.K. and S.L.; project administration, S.W.K.; supervision, S.W.K.; writing—original draft, S.W.K. and W.-S.K.; writing—review and editing, S.W.K. and S.L. All authors have read and agreed to the published version of the manuscript.

**Funding:** This work was financially supported by grants from the Korea Institute of Geoscience and Mineral Resources (GP2021-004), funded by the Ministry of Science, Information, Communication and Technology.

**Institutional Review Board Statement:** Not applicable.

**Informed Consent Statement:** Not applicable.

**Data Availability Statement:** Not applicable.

**Acknowledgments:** We thank D.H. Kim at the Hanil Nuclear Power Co., Ltd. for assistance with gamma nuclide analysis. Three anonymous reviewers are thanked for their insightful suggestions and comments, which improved the quality of this manuscript.

**Conflicts of Interest:** The authors declare no conflict of interest.

## References

1. Mason, B.; Moore, C.B. *Principles of Geochemistry*, 4th ed.; John Wiley: New York, NY, USA, 1982.
2. Hwang, J. Occurrence of U-minerals and source of U in Groundwater in Daebo granite, Daejeon area. *J. Eng. Geol.* **2013**, *23*, 399–407, (In Korean with English abstract). [[CrossRef](#)]
3. Kim, M.S.; Kim, T.S.; Kim, H.K.; Kim, D.S.; Jeong, D.H.; Ju, B.K.; Hong, J.K.; Kim, H.J.; Park, S.H.; Jeong, C.H.; et al. Study on temporal decay characteristics of naturally occurring radionuclides in groundwater in two mica granite area. *J. Soil Groundw. Environ.* **2013**, *18*, 19–31, (In Korean with English abstract). [[CrossRef](#)]
4. Yun, S.W.; Lee, J.; Park, Y. Occurrence of radionuclides in groundwater of Korea according to geologic condition. *J. Eng. Geol.* **2016**, *26*, 71–78, (In Korean with English abstract). [[CrossRef](#)]
5. Hwang, J. Geological Review on the distribution and source of uraniumiferous groundwater in South Korea. *J. Eng. Geol.* **2018**, *28*, 593–603, (In Korean with English abstract).
6. Kim, S.W. Concentration of Radioactive Materials for the Phanerozoic Plutonic Rocks in Korea and Its Implication. *Econ. Environ. Geol.* **2020**, *53*, 565–583, (In Korean with English abstract).
7. Hwang, J.; Moon, S.-H. Geochemistry of U and Th of Mesozoic granites in South Korea: Implications of occurrences of different U-host minerals and dissolved U and Rn between Jurassic and Cretaceous granite aquifers. *Geosci. J.* **2021**, *25*, 183–195. [[CrossRef](#)]
8. Kee, W.S.; Kim, S.W.; Jeong, Y.J.; Kwon, S. Characteristics of Jurassic continental arc magmatism in South Korea: Tectonic implications. *J. Geol.* **2010**, *118*, 305–323. [[CrossRef](#)]
9. Kim, S.W.; Kwon, S.; Koh, H.J.; Yi, K.; Jeong, Y.; Santosh, M. Geotectonic framework of Permo-Triassic magmatism within the Korean Peninsula. *Gondwana Res.* **2011**, *20*, 865–889. [[CrossRef](#)]

10. Kim, S.W.; Kwon, S.; Koh, K.; Yi, K.; Cho, D.-L.; Kee, W.-S.; Kim, B.C. Geochronological and geochemical implications of Early to Middle Jurassic continental adakitic arc magmatism in the Korean Peninsula. *Lithos* **2015**, *227*, 225–240. [[CrossRef](#)]
11. Kee, W.S.; Kim, S.W.; Hong, P.S.; Lee, B.C.; Cho, D.R.; Byun, U.H.; Ko, K.; Kwon, C.W.; Kim, H.C.; Jang, Y.; et al. *Geologic Map of Korea (1:1,000,000)*; Korea Institute of Geoscience and Mineral Resources: Daejeon, Korea, 2019.
12. Oh, C.W.; Lee, B.C.; Yi, S.; Ryu, H.I. Correlation of Paleoproterozoic igneous and metamorphic events of the Korean Peninsula and China; Its implication to the tectonics of Northeast Asia. *Precambrian Res.* **2019**, *326*, 344–362. [[CrossRef](#)]
13. Cheong, A.C.; Jo, H.J. Tectonomagmatic evolution of a Jurassic Cordilleran flare-up along the Korean Peninsula: Geochronological and geochemical constraints from granitoid rocks. *Gondwana Res.* **2020**, *88*, 21–44. [[CrossRef](#)]
14. Cho, D.L.; Lee, B.C.; Oh, C.W. Petrogenesis of Paleoproterozoic (2.02–1.96 Ga) metagranitoids in the southwestern Yeongnam Massif, Korean Peninsula, and their significance for the tectonic history of northeast Asia: Insights from zircon U–Pb–Hf isotope and whole-rock geochemical compositions. *Precambrian Res.* **2020**, *340*, 105631.
15. Kim, S.W.; Kwon, S.; Jeong, Y.-J.; Kee, W.-S.; Lee, B.C.; Byun, U.H.; Ko, K.; Cho, D.-L.; Hong, P.S.; Park, S.-I.; et al. The Middle Permian to Triassic tectono-magmatic systems in the southern Korean Peninsula. *Gondwana Res.* **2020**, in press. [[CrossRef](#)]
16. Wilson, M. Magmatic differentiation. *J. Geol. Soc.* **1993**, *150*, 611–624. [[CrossRef](#)]
17. Cuney, M. Uranium and thorium: The extreme diversity of the resources of the world's energy minerals. In *Non-Renewable Resource Issues*; Springer: Dordrecht, The Netherlands, 2012; pp. 91–129.
18. Cuney, M. Felsic magmatism and uranium deposits. *Bull. Soc. Geol. Fr.* **2014**, *185*, 75–92. [[CrossRef](#)]
19. Gelman, S.E.; Deering, C.D.; Bachmann, O.; Huber, C.; Gutiérrez, F.J. Identifying the crystal graveyards remaining after large silicic eruptions. *Earth Planet. Sci. Lett.* **2014**, *403*, 299–306. [[CrossRef](#)]
20. *Guidelines on the Radon Reduction and Management of Construction Material*; Joint Ministries (Ministry of Environment, Ministry of Land, Infrastructure and Transport, and Nuclear Safety Committee): Sejong City, Korea, 2019; p. 21. (In Korean)
21. EC (European Commission). *Radiation Protection 112—Radiological Protection Principles Concerning the Natural Radioactivity of Building Materials*; European Commission: Luxembourg, 1999; ISBN 92-828-8376-0.
22. Kim, K.-B.; Chwae, U.; Hwang, J.H.; Kim, J.H. *Geological Report of the Osu Sheet (1:50,000)*; Korea Institute of Geology, Mining and Materials: Daejeon, Korea, 1984; p. 38, (In Korean with English summary).
23. Hong, S.H.; Yun, W. *Geological Report of the Changkye Sheet (1:50,000)*; Korea Institute of Geology, Mining and Materials: Daejeon, Korea, 1993; p. 17, (In Korean with English summary).
24. Kim, K.-B.; Chwae, U. *Geological Report of the Hamyang Sheet (1:50,000)*; Korea Institute of Geology, Mining and Materials: Daejeon, Korea, 1994; p. 16, (In Korean with English summary).
25. Paton, C.; Woodhead, J.D.; Hellstrom, J.C.; Hergt, J.M.; Greig, A.; Maas, R. Improved laser ablation U–Pb zircon geochronology through robust downhole fractionation correction. *Geochem. Geophys. Geosyst.* **2010**, *11*, Q0AA06. [[CrossRef](#)]
26. Paton, C.; Hellstrom, J.; Paul, B.; Woodhead, J.; Hergt, J. Iolite: Freeware for the visualization and processing of mass spectrometric data. *J. Anal. At. Spectrom.* **2011**, *26*, 2508–2518. [[CrossRef](#)]
27. Ludwig, K.R. *User's Manual for Isoplot 3.6: A Geochronological Toolkit for Microsoft Excel*; Berkeley Geochronology Center Special Publication 2008; Berkeley Geochronology Center: Berkeley, CA, USA, 2008.
28. Ludwig, K.R. *User's Manual for SQUID 2*; Berkeley Geochronology Center Special Publication 2009; Berkeley Geochronology Center: Berkeley, CA, USA, 2009.
29. Middlemost, E.A.K. Naming materials in the magma/igneous rock system. *Earth Sci. Rev.* **1994**, *37*, 215–224. [[CrossRef](#)]
30. Shand, S.J. *The Erutite Rocks: Their Genesis, Composition, and Classification, with a Chapter on Meteorites*, 2nd ed.; John Wiley & Sons: New York, NY, USA, 1947; 444p.
31. Sun, S.; McDonough, W.F. Chemical and isotopic systematics of oceanic basalts: Implications for mantle composition and processes Basins. In *Magmatism in the Ocean Basins*; Saunders, A.D., Norry, M.J., Eds.; Special Publications 42; Geological Society of London: London, UK, 1989; pp. 313–345.
32. Pearce, J.A.; Harris, N.B.W.; Tindle, A.G. Trace element discrimination diagrams for the tectonic interpretation of granitic rocks. *J. Petrol.* **1984**, *25*, 956–983. [[CrossRef](#)]
33. Bateman, P.C.; Chappell, B.W. Crystallization, fractionation, and solidification of the Tuolumne intrusive series, Yosemite National Park, California. *Geol. Soc. Am. Bull.* **1979**, *90*, 465–482. [[CrossRef](#)]
34. Ballouard, C.; Poujol, M.; Boulvais, P.; Branquet, Y.; Tartèse, R.; Vigneresse, J.L. Nb-Ta fractionation in peraluminous granites: A marker of the magmatic-hydrothermal transition. *Geology* **2016**, *44*, 231–234. [[CrossRef](#)]
35. David, A.W.; Calvin, F.M. Accessory mineral behavior during differentiation of a granite suite: Monazite, xenotime and zircon in the Sweetwater Wash pluton, southeastern California, USA. *Chem. Geol.* **1993**, *110*, 49–67.
36. Karel, B. Monazite and zircon as major carriers of Th, U, and Y in peraluminous granites: Examples from the Bohemian Massif. *Miner. Petrol.* **2016**, *110*, 767–785.